Comparative analysis of the near-anode and near-cathode boundary layers in high-pressure arc discharges

N. A. Almeida and M. S. Benilov

Departamento de Física, Universidade da Madeira, 9000 Funchal, Portugal

Numerical investigation of near-anode and near-cathode layers of very high-pressure arcs in mercury and xenon is reported. The simulation is performed by means of a recently developed numerical model in which the whole of a near-electrode layer is simulated in the framework of a single set of equations without simplifying assumptions such as thermal equilibrium, ionization equilibrium, and quasi-neutrality. The system of equations includes equations of conservation of each species (the atoms, ions and electrons), transport equations for each species, equation of energy of the heavy species (the atoms and ions), equation of energy of the electrons, and the Poisson equation. The system of equations is solved numerically in 1D. The approach being used allows one to model the near-cathode and near-anode layer by means of the same code. The obtained results clearly show the same structure for the near-cathode and near-anode layer.

1. Introduction

The plasma-electrode interaction in high-pressure arc discharges is dominated by non-LTE effects (e.g., [1] and references therein), which include a violation of thermal equilibrium, i.e., a divergence between the electron and heavy-particle temperatures; a violation of ionization equilibrium, i.e., a deviation of the charged-particle density from that predicted by the Saha equation; and a violation of quasi-neutrality, i.e., a divergence between the electron and ion number densities. A straightforward numerical calculation of near-electrode plasma layers with account of all these effects represents a difficult task. Therefore, in most works either some of these effects are discarded (e.g., [2–7]), or the near-electrode layer is *a priori* divided into a number of sub-layers, such as a layer of thermal non-equilibrium, an ionization layer, a near-electrode space-charge sheath, *etc*, with each sub-layer being described by a separate set of equations and solutions in adjacent sub-layers being matched in some way or other at a boundary between the sub-layers (e.g., [1] and references therein).

Papers in which the whole of a near-electrode layer is simulated in the framework of a single set of equations with account of all the above-mentioned non-LTE effects have started to appear only recently [8–10]. Such unified modelling approach does not rely on intuitive considerations, which are inevitable in models based on sub-layers and differ from one model to another, and is useful for developing commonly accepted physical understanding and/or simulation methods. This approach, at least

in principle, is independent of polarity and allows one to model both near-cathode and near-anode layers by means of the same code by merely changing sign of the current density; a feature important from the methodical point of view and essential for modelling near-electrode layers of AC arcs. In this work a comparative analysis of the near-anode and near-cathode boundary layers in high-pressure arc discharges is reported. The analysis is performed for plasmas of xenon and mercury under conditions typical of very high-pressure discharge lamps.

2. Modelling

The simulations have been performed by means of the model [9,10]. The model takes into account the neutral atoms, ions, and electrons; the atoms and ions have the same temperature T_h which is in general different from the electron temperature T_e. The system of equations includes equations of conservation of each species, transport equations for each species, equation of energy of the heavy species (the atoms and ions), equation of energy of the electrons, and the Poisson equation. The transport equations for species are written in the form of hydrodynamic Stefan-Maxwell equations (e.g., [11,12] and references therein), which are applicable at any ionization degree of the plasma, in contrast to a description based on Fick's law for the ions and the electrons which is valid provided that the ionization degree is low enough.

The modelling results reported in this work refer to the case of parallel-plane current transfer to a planar electrode through a planar near-electrode region. The independent variable is x the distance

measured from the electrode surface into the plasma. The electric current density j is the same at all points of the plasma in the planar case and is considered as an input parameter, $j > 0$ corresponding to the case of anode and $j < 0$ to the case of cathode.

The boundary conditions at the electrode surface, $x = 0$, are the same as in [9] and take into account the emission of electrons by the surface. Since the current density is constant in the planar geometry, all parameters of the plasma (except the electrostatic potential) are constant at large distances from the electrode, where the plasma is close to the state of local thermodynamic equilibrium, or LTE, and its energy balance is dominated by radiation. One can say that the plasma far from the electrode is not disturbed by the electrode. The upper boundary of the calculation domain, $x = L$, in the planar case is positioned in the undisturbed plasma and the conditions at this boundary are zero derivatives [10].

Three input parameters must be specified for each plasma-producing gas: the density of electric current, j, the temperature of the electrode surface, and the value of plasma pressure at $x = L$, i.e., in the undisturbed plasma.

3. Results

Distributions of parameters in the near-electrode non-equilibrium layer are shown in figures 1-8. Figures 1-4 refer to xenon, and figures 5-8 refer to mercury. The temperature of the electrode surface was set equal to $3000\,\mathrm{K}$ and the plasma pressure in the undisturbed plasma was fixed at $100\,\mathrm{bar}$. The electrode in the simulations was assumed to be made of pure tungsten. The parameters shown include: densities of the ions and the electrons n_i and n_e, electron and heavy-particle temperatures T_e and T_h, and the projection E of the electric field over the x-axis. Also shown is n_S, the charged-particle density evaluated by means of the Saha equation in terms of the local heavy-particle and electron temperatures and with the local plasma pressure equal to the pressure in the undisturbed plasma.

Although the data plotted in figures 1-8 have been obtained by modelling the whole of the non-equilibrium layer by means of a single set of equations, i.e., without dividing it into different sub-layers, the modelling results clearly reveal regions dominated by different physical processes. In figures 1 and 2, vertical dashed lines are used to separate adjacent sub-layers (these separation lines are shown for illustrative purposes only; of course no
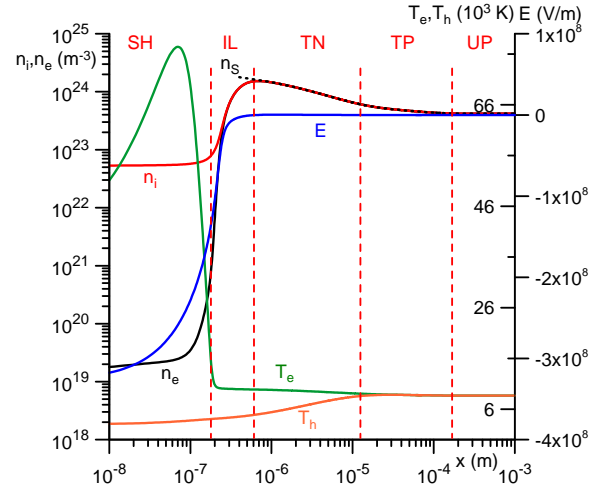
Figure 1: Distribution of parameters in the near-cathode non-equilibrium layer. Xe plasma, $j = -10^7\,\mathrm{A/m^2}$.
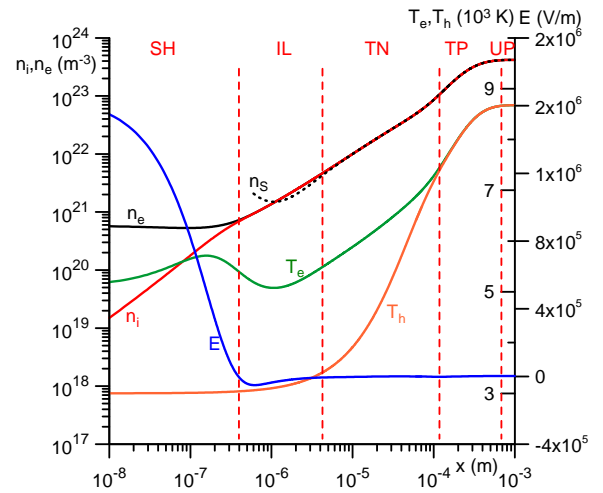
Figure 2: Distribution of parameters in the near-anode non-equilibrium layer. Xe plasma, $j = 10^7\,\mathrm{A/m^2}$.

distinct boundaries between different sub-layers exist in reality). One can identify the following regions: the space-charge sheath (SH), the ionization layer (IL), the layer of thermal non-equilibrium (TN), the layer of thermal perturbation (TP), and the region of undisturbed plasma (UP).

One can see that the structure of the near-cathode and near-anode layer is similar. In contrast to what happens in the case of Xe, the results of the modelling for Hg do not reveal an ionization layer. As the current density increases, thickness of the near electrode layer decreases. For instance, for the conditions of figure 1 ($j = -10^7\,\mathrm{A/m^2}$), the thickness of the near-cathode layer is around $2\times10^{-4}\,\mathrm{m}$, while for the conditions of figure 3 ($j = -10^8\,\mathrm{A/m^2}$) the thickness is around $10^{-5}\,\mathrm{m}$. In the case of the near-anode layer the decrease in the thickness with the
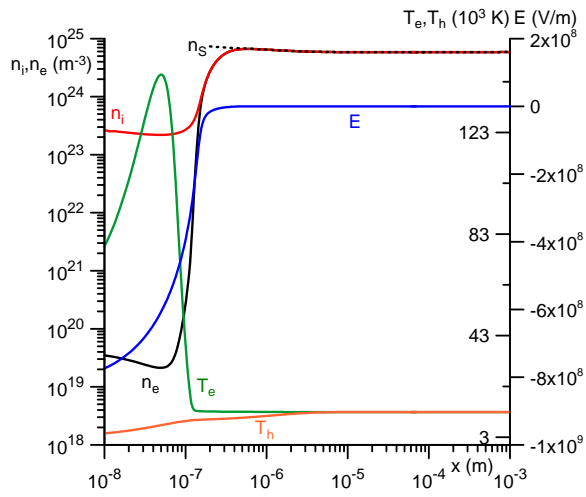
Figure 3: Distribution of parameters in the near-cathode non-equilibrium layer. Xe plasma, $j = -10^8 \, \text{A/m}^2$.
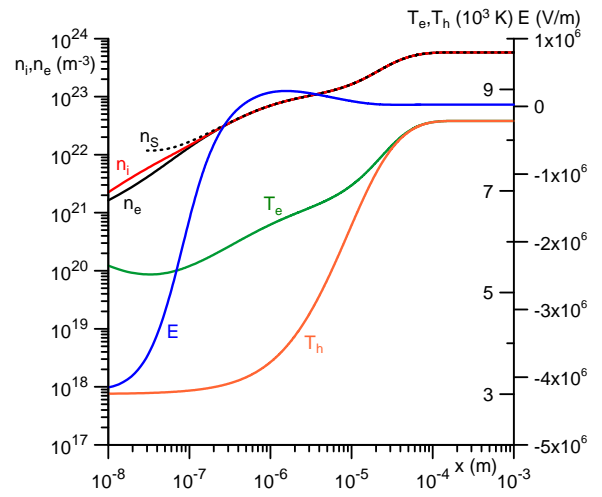
Figure 6: Distribution of parameters in the near-anode non-equilibrium layer. Hg plasma, $j = 10^7 \, \text{A/m}^2$.
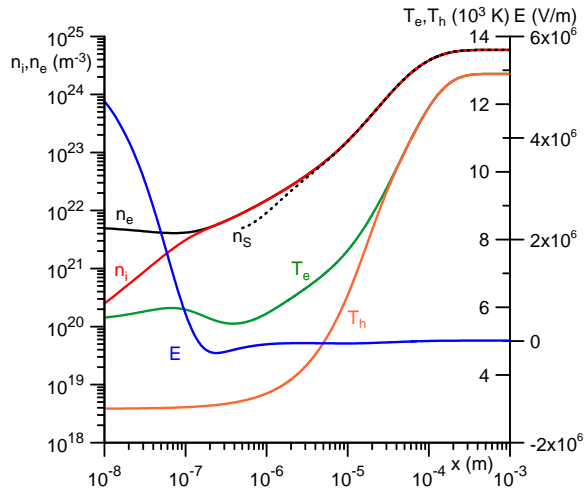
Figure 4: Distribution of parameters in the near-anode non-equilibrium layer. Xe plasma, $j = 10^8 \, \text{A/m}^2$.
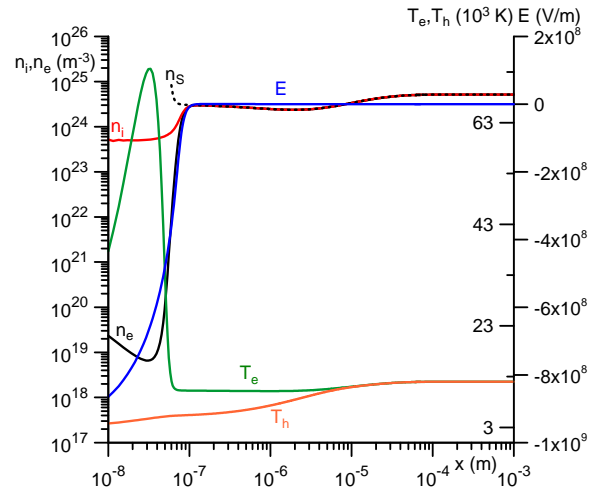
Figure 7: Distribution of parameters in the near-cathode non-equilibrium layer. Hg plasma, $j = -10^8 \, \text{A/m}^2$.
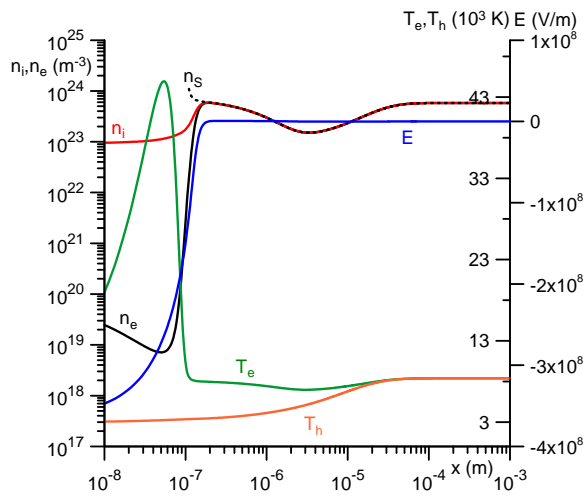
Figure 5: Distribution of parameters in the near-cathode non-equilibrium layer. Hg plasma, $j = -10^7 \, \text{A/m}^2$.
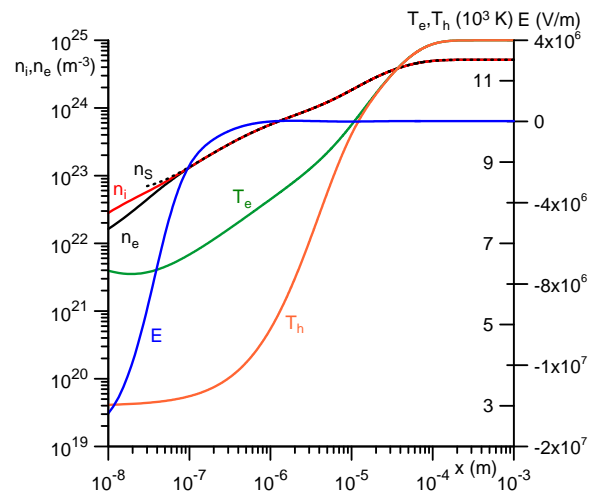
Figure 8: Distribution of parameters in the near-anode non-equilibrium layer. Hg plasma, $j = 10^8 \, \text{A/m}^2$.

increase in the current density is much less pronounced. For instance, for the conditions of figure 2 ($j = 10^7\,\mathrm{A/m^2}$), the thickness of the near-anode layer is around $7 \times 10^{-4}\,\mathrm{m}$, while for the conditions of figure 4 ($j = 10^8\,\mathrm{A/m^2}$) the thickness is around $4 \times 10^{-4}\,\mathrm{m}$. Hence the effect in the case of the cathode is stronger than in the case of the anode. For Hg the results are similar.

There is a maximum of the electron temperature inside the space-charge sheath in all the near-cathode layers (figures 1, 3, 5 and 7). The reason of the appearance of this maximum was already studied in [9]: it was found that it is manifestation of a strong supply of energy to the electron gas in the space-charge sheath, that occurs in the cases where the ratio of the emission current to the total current is below or slightly above unity and makes possible the generation of an ion current necessary to compensate the deficit of the electron current.

For conditions of figures 6 and 8, the ion density n_i in the sheath exceeds the electron density n_e and the electric field in the sheath is negative, i.e., directed to the electrode surface. This situation is typical for near-cathode layers but occurs frequently also in near-anode layers, namely, in cases where the plasma density near the anode is higher than that needed to provide transport of the arc current to the anode and a part of plasma electrons must be prevented from entering the sheath; see, e.g., the discussion and references in [13] and the estimates in [1].

4. Conclusions

In this work a comparative analysis of the near-anode and near-cathode boundary layers in high-pressure arc discharges in xenon and mercury is performed. The employed approach allows one to model the near-electrode region in a unified way without any simplifying assumptions. It also permits one to model near-cathode and near-anode layer by means of the same code. The obtained results clearly show that the structure of the near-cathode and near-anode layer is similar. A significant decrease of the thickness of the near-cathode layer with increasing current density is observed. For the near-anode layer the effect is less pronounced.

5. References

[1] M. S. Benilov, J. Phys. D: Appl. Phys. **41** (2008) 144001.

[2] T. Amakawa, J. Jenista, J. V. R. Heberlein, and E. Pfender, J. Phys. D: Appl. Phys. **31** (1998) 2826.

[3] J. Haidar, J. Phys. D: Appl. Phys. **32** (1999) 263.

[4] F. Lago, J. J. Gonzalez, P. Freton, and A. Gleizes, J. Phys. D: Appl. Phys. **37** (2004) 883.

[5] P. Flesch and M. Neiger, J. Phys. D: Appl. Phys. **38** (2005) 3098.

[6] R. Bini, M. Monno, and M. I. Boulos, J. Phys. D: Appl. Phys. **39** (2006) 3253.

[7] J. J. Lowke and M. Tanaka, J. Phys. D: Appl. Phys. **39** (2006) 3634.

[8] A. Lenef, L. Dabringhausen, and M. Redwitz, in Proceedings of the 10th International Symposium on the Science and Technology of Light Sources, Toulouse, 2004, G. Zissis, Ed. Bristol: Institute of Physics, 2004, 429.

[9] N. A. Almeida, M. S. Benilov, and G. V. Naidis, J. Phys. D: Appl. Phys. **41** (2008) 245201.

[10] N. A. Almeida, M. S. Benilov, U. Hechtfischer, and G. V. Naidis, J. Phys. D: Appl. Phys. **42** (2009) 045210.

[11] V. M. Zhdanov, Transport Phenomena in Multicomponent Plasma. London and New York: Taylor and Francis, 2002.

[12] V. Rat, A. B. Murphy, J. Aubreton, M. F. Elchinger, and P. Fauchais, J. Phys. D: Appl. Phys. **41** (2008) 183001.

[13] M. Redwitz, L. Dabringhausen, S. Lichtenberg, O. Langenscheidt, J. Heberlein, and J. Mentel, J. Phys. D: Appl. Phys. **39** (2006) 2160.